Proceedings of the 2008 International Manufacturing Science and Engineering Conference
MSEC2008
October 7-10, 2008, Evanston, Illinois, USA

MSEC_ICM&P2008-72514

SPATIALLY RESOLVED CHARACTERIZATION OF GEOMETRICALLY NECESSARY DISLOCATION DEPENDENT DEFORMATION IN MICRO- SCALE LASER SHOCK PEENING

Youneng Wang
Dept. of Mechanical Engineering
Columbia University
New York, NY 10027
yw2119@columbia.edu

Sinisa Vukelic
Dept. of Mechanical Engineering
Columbia University
New York, NY 10027
sv2147@columbia.edu

Jeffrey W. Kysar
Dept. of Mechanical Engineering
Columbia University
New York, NY 10027
jk2079@columbia.edu

Y. Lawrence Yao
Dept. of Mechanical Engineering
Columbia University
New York, NY 10027
yly1@columbia.edu

ABSTRACT

As the laser spot size in micro-scale laser shock peening is in the order of magnitude of several microns, the anisotropic response of grains will have a dominant influence on its mechanical behavior of the target material. Furthermore, conventional plasticity theory employed in previous studies needs to be reexamined due to the length scale effect. In the present work, the length scale effects in microscale laser shock peening have been investigated. The crystal lattice rotation underneath the shocked surface was determined via Electron Backscatter Diffraction (EBSD). From these measurements, the geometrically necessary dislocations (GND) density that the material contains has been estimated. The yield strength increment was then calculated from the GND distribution by using Taylor model and integrated into each material point of the FEM simulation. Finite element simulations, based on single crystal plasticity, were performed of the process for both with and without considering the GND hardening and the comparison has been conducted.

INTRODUCTION

Micro-scale laser shock peening (μLSP), which aims to improve fatigue performance by imparting a compressive residual stress into the target material surface layer using laser induced shock waves, has been the focus of several recent investigations [1, 2]. This process is desirable for metallic components of micro-devices which encounter cyclic loading, such as micro-switches, micro-blades of a micro turbine, etc. Previous work has shown [1, 2] through both numerical analysis and experiments that through μLSP, one can manipulate the compressive residual stress distribution in a region close to the shocked surface with micron spatial resolution.

Recent experiments in both bending and indentation have shown that the apparent material hardening increases as the size of specimen decreases to micron level [3, 4] where classical plasticity theory has been unable to account for the observed phenomena. It is well known now [5, 6, 7] that this hardening is due to length scale effects. Therefore, when the laser beam spot size is reduced to several microns, i.e. the same order of grain size, the size scale will have significant influence on mechanical behavior and the conventional plasticity theory must be reexamined as well. However, the numerical models developed before [1, 2] to predict the material response to the μLSP process are simplified and approximated without considering length scale effects and all based on the conventional plasticity theory. In order to better understand μLSP process and more accurately simulate the process, it is necessary to understand the length scale effect on the process and integrate this into the simulation model.

In micro-scale deformation, strain gradient effects may be large enough such that the yield strength of a material depends not only on the strain, but also on the strain gradient. The motivation behind the use of strain gradients is based on the framework of geometrically necessary dislocations (GNDs), which were first introduced by Nye [8] and furthered by Ashby [9], who have given a physical basis for strain gradient dependent material behavior. Strain gradient theories have been physically motivated by developments in dislocation mechanics. More details about geometrically necessary

dislocations in single crystals and polycrystalline materials can be found in Arsenlis and Parks [6]. In particular, several strain gradient models have been developed to numerically capture length scale effects where the underlying physics is sometimes related to the geometrically necessary dislocation [5, 10].

There have been a number of investigations on geometrically necessary dislocation density under constant loading or punch configurations for anisotropic materials [11, 12]. For example, Kysar et al. [12] estimated the distribution of geometrically necessary dislocation density on a cross section of a wedge indented aluminum single crystal via EBSD measurement. As lattice curvature induced by μLSP is relatively small compared with those of a constant load or a punch, length scale effects are not obvious in μLSP and can not simply be copied from their works. The objective of the present work is to find the spatial distribution of the geometrically necessary dislocation density after μLSP process from both numerical and experimental results for single crystal aluminum under plane strain condition. Gaussian pressure loading, corresponding to the pressure caused by laser shock peening, was assumed in the numerical simulation and the resulting plastic deformation was analyzed to find the distribution of the geometrically necessary dislocation density.

The remainder of the chapter is organized as follows. Section 2 gives details about experimental conditions and post-peening material characterization, which includes lattice rotation quantification by EBSD. Principles of the evaluation of geometrically necessary dislocations density are described in Section 3. In Section 4, finite element simulation employed to study the length scale effect in the target material after μLSP is presented. Section 5 gives the results and discussion. Following are concluding marks.

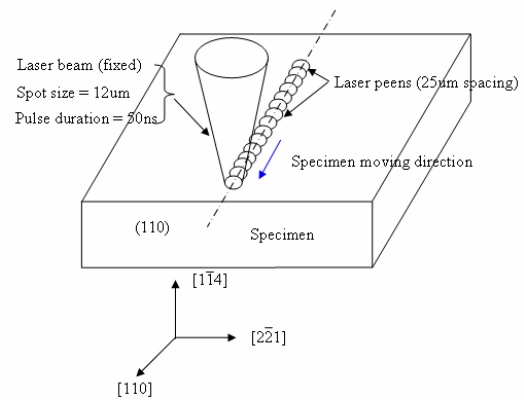

Fig. 1 Experimental set-up

EXPERIMENTAL CONDITIONS AND POST-PEENING MATERIAL CHARACTERIZATION

A frequency tripled Q-switched Nd:YAG laser ($\lambda = 355\,nm$) in TEM_{00} mode was used for the μLSP experiments with a 50ns pulse duration and a 12μm beam diameter, as shown in Fig. 1. A thin layer of high vacuum grease (about 10 microns thick) was spread evenly on the sample surface, and a 16μm thick polycrystalline aluminum foil, chosen for its relatively low threshold of vaporization, was tightly pressed onto the grease. The sample was placed in a shallow container filled with distilled water approximately 3 mm above the sample's top surface. A line of μLSP shocks were created on the sample surface with a 25 μm spacing along the [110] direction as shown in Fig. 1. A pulse energy of 228μJ was used which corresponded to a laser intensity of 4.03GW/cm^2. After shock processing, the coating layer and the vacuum grease were manually removed.

A single crystal aluminum with the orientation $(1\bar{1}4)$ is chosen because when shocks applied along $[110]$ direction approximate plane strain condition is achieved [13] and under the Gaussian pressure loading only one slip system is activated. Furthermore, aluminum is a popular material used in micro metallic devices so it is of interest to study its mechanical behavior under μLSP. In preparation for laser shock peening, the sample surface was polished mechanically by using grit 600 sand paper and then repeated by using grit 1200 sand paper. After sandpaper polish, the specimen was polished using diamond paste with lapping oil as a lubricant, first 6 μm paste and then 1μm with minimum pressure was used until no directionally preferential scratches were visible under optical microscope with 100x magnification. In order to remove any residual stress induced during the mechanical polish process, the sample was electro-polished before shocking.

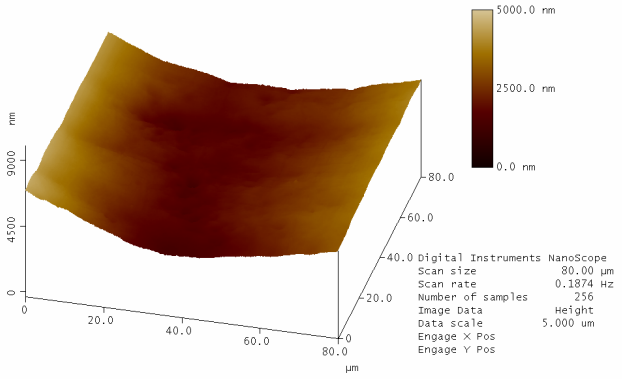

Fig. 2 Deformed geometry of shocked line by using SPM with scan area=80×80μm and data scale=1μm

The shocked region was measured using scanning probe microscopy (SPM, Digital Instruments Nanoscope Inc.) as shown in Fig. 2 for a scanning area of 80μm×80μm. After the shock peening, EBSD data was collected using a system supplied by HKL Technology and attached to a JEOL JSM 5600LV scanning electron microscope (SEM). All data were acquired in the automatic mode, using external beam scanning and employing a 3μm step size as the preliminary investigation revealed negligible levels of orientation difference at finer scales of inquiry. The scan area chosen was 150μm(width)×100μm(depth) on the cross section as the effected area by μLSP is usually smaller than this area. The EBSD results from each individual scan comprise data containing the position coordinates and the three Euler angles which describe the orientation of the particular interaction volume relative to the orientation of the specimen in the SEM allowing in-plane and out-of-plane lattice rotations to be calculated relative to the known undeformed crystallographic orientation, which serves as a reference state.

EVALUATION OF GEOMETRICALLY NECESSARY DISLOCATION DENSITY AND ITS HARDENING EFFECT

Based on the work by Kysar et al. [12], the evaluation principles of the geometrically necessary dislocation density are briefly summarized here as follows. First, the lattice curvature, global coordinate x, y, z and local coordinate systems x', y' and z' are defined as shown in Fig. 3. By naming the lattice rotation about the *x*, *y* and *z* coordinates as ω_1, ω_2 and ω_3, respectively, the crystal lattice curvature tensor, κ_{ij} can be described as [8]:

$$\kappa = \begin{pmatrix} \kappa_{11} & \kappa_{12} & \kappa_{13} \\ \kappa_{21} & \kappa_{22} & \kappa_{23} \\ \kappa_{31} & \kappa_{32} & \kappa_{33} \end{pmatrix} \tag{1}$$

where $\kappa_{ij} = \dfrac{\partial \omega_i}{\partial x_j}$. Under plane strain condition, $\omega_1 = 0$, $\omega_2 = 0$. ω_3 can be found through EBSD measurement. According to Nye's dislocation tensor [8], α_{ij}, which is a representation of dislocation with Burgers vector *i* and line vector *j*, α_{ij} can be described as [12]:

$$\alpha_{ij} = \sum_{n=1}^{m} \rho^{(n)} b_i^{(n)} t_i^{(n)} \tag{2}$$

where *n* is an integer, *m* the total number of active slip systems, $t_j^{(n)}$ is the tangent line vector of dislocation which also is a unit vector but its direction is perpendicular to the (110) plane, $b_i^{(n)}$ is the effective length of Burgers vector of the slip system *n*, $\rho^{(n)}$ is the density of geometrically necessary dislocations on slip system *n*.

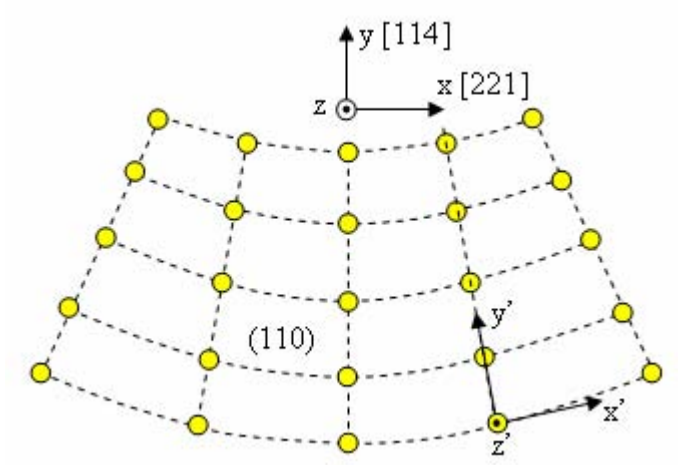

Fig. 3 The crystal lattice curvature and coordinate system

Assuming the elastic strain gradient is negligible compared to the lattice rotation gradient, Nye's tensor is related to the lattice curvature tensor as [6]:

$$\kappa_{ij} = -\alpha_{ji} + \frac{1}{2}\delta_{ji}\alpha_{kk} \tag{3}$$

where δ_{ji} is the Kronecker delta. Considering the plane strain condition, Nye's dislocation density tensor in local coordinate can be described as

$$\alpha' = \begin{pmatrix} 0 & 0 & \alpha_{13}\cos\omega_3 + \alpha_{23}\cos\omega_3 \\ 0 & 0 & -\alpha_{13}\cos\omega_3 + \alpha_{23}\cos\omega_3 \\ 0 & 0 & 0 \end{pmatrix} \tag{4}$$

Following the work of Kysar et al. [12],

$$\alpha'_{ij} = \sum_{n=1}^{3} \rho^{(n)} b^{(n)} s_i^{(n)} t_j^{(n)} \tag{5}$$

for the plane strain condition with three effective slip systems, where $s_i^{(n)}$ is a unit vector in the slip direction which is parallel to the Burgers vector, and *n* takes value of 1, 2, or 3, depending on the active slip system.

The above is a brief summary of the GND evaluation principles employed in this paper. It should be pointed out that there are differences between Kysar et al. [12] and the presented work. Kysar et al. [12] employed the above evaluation to characterize the GND induced by wedge indentation on a single crystal aluminum with low index orientation [001], which corresponds to symmetrical deformation with respect to the yield surface. Also, Kysar et al. [12] yielded only an estimate of GND density, not the actual density. In this paper, single crystal aluminum with orientation $[1\bar{1}4]$ corresponding to asymmetrical deformation is used since it only has a single slip system activated in the main regions of plastic deformation under plane strain conditions. Therefore, the induced GND will be smaller than that of [001] or other symmetrical orientations under the same conditions as there are two active slip systems for these orientations. Thus, if the hardening caused by GND for the orientation $[1\bar{1}4]$ can not be neglected, it follows that it cannot be ignored for symmetrical orientations either.

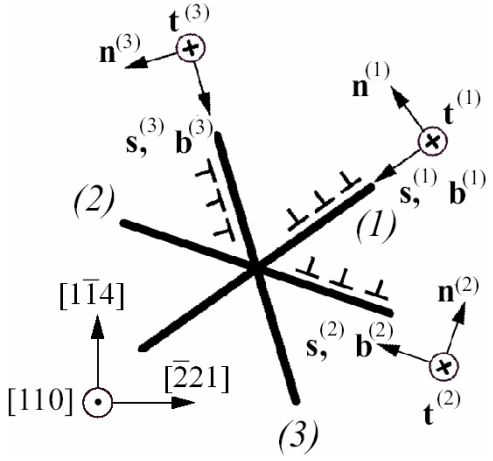

Fig. 4 The three effective slip systems in the aluminum single crystal of $[1\bar{1}4]$ orientation

Based on Eq. (5), the geometric parameters $s_i^{(n)}$ and $t_j^{(n)}$ are different from the [001] and must be determined first. From Fig. 4, the parameters can be found according to the geometrical relationship listed in Table 1.

Table 1: Geometrically necessary dislocation parameters of FCC crystals for Al $[1\bar{1}4]$ sample

Slip system	Slip angle	Unit vector of slip: **s**	Dislocation line vector: **t**
(1)	-35.3°	$\left(-\sqrt{\frac{2}{3}},\ -\sqrt{\frac{1}{3}},\ 0\right)$	(0, 0, -1)
(2)	-19.4°	$\left(-\frac{2}{3}\sqrt{2},\ \frac{1}{3},\ 0\right)$	(0, 0, -1)
(3)	-74.1°	$\left(\frac{1}{3}\sqrt{\frac{2}{3}},\ -\frac{5}{3}\sqrt{\frac{1}{3}},\ 0\right)$	(0, 0, -1)

By applying the unit vectors and dislocation line vectors, Eq.(5) can be written as

$$\alpha'_{13} = \rho^{(1)}b^{(1)}\sqrt{\frac{1}{3}} + \rho^{(2)}b^{(2)} - \rho^{(3)}b^{(3)}\sqrt{\frac{1}{3}} \quad (6a)$$

$$\alpha'_{23} = \rho^{(1)}b^{(1)}\sqrt{\frac{2}{3}} + \rho^{(3)}b^{(3)}\sqrt{\frac{2}{3}} \quad (6b)$$

For the two equations with three unknowns, a solution may be found by optimizing the variables in a certain sense, such as the least norm solution by minimizing $\left\{\left[\rho^{(1)}\right]^2 + \left[\rho^{(2)}\right]^2 + \left[\rho^{(3)}\right]^2\right\}^{1/2}$ through singular value decomposition [6]. By summing the density of each slip system, the total GND density can be found. The approximate strength of the single crystal in the shocked region can be calculated using the Taylor hardening model in which the yield strength of a material, σ_y is proportional to the square root of the geometrically necessary dislocation density $\sqrt{\rho}$. By assuming that all slip systems harden at the same rate, the enhanced strength is related to the square root of GND [9]:

$$\tau = c\mu b\sqrt{\rho} \quad (7)$$

where c is a constant related to the crystal and grain structure, usually ranging from 0.1 to 0.5 [9], τ is the enhanced flow stress by GND in each slip system, μ is shear modulus, b is the Burger's vector and ρ is the total GND density.

FINITE ELEMENT SIMULATION OF SPATIALLY RESOLVED GND DEPENDENT DEFORMATION

In order to estimate length scale effects on micro-scale laser shock peening, a simulation strategy depicted by the flow chart in Fig. 5 is followed. First, based on the evaluation principles discussed above, the geometrically necessary dislocation density is found according to Eqs. (6a) and (6b) from lattice rotation of the simulation without considering length scale effects and is validated by the experimental result of EBSD measurement. Then, the enhanced strength due to the geometrically necessary dislocations is calculated at each material point or node in finite element simulation by using Eq. (7). The current strength in each step is updated by combining the local enhanced strength with the global initial strength. The enhanced strength is applied in a linear manner; that is, it increases from zero to the final strength during the loading step and remains constant in the relaxation step as the plastic deformation is unrecoverable during the relaxing.

In the simulation, the theory of single crystal plasticity [14] was integrated into finite element simulation by a user-material subroutine (UMAT), written by Huang [15] and modified by Kysar [16]. It is incorporated into the finite element analysis using the general purpose finite element program ABAQUS/Standard. In the UMAT, the {111}<110> slip systems in FCC metal are employed and an initial critical resolved shear strength $\tau_{CRSS} \approx 1MPa$ is assumed for each of the slip systems, which is a reasonable value for high purity single crystals employed (e.g. [17]). The element used in the simulation was plane strain reduced integration, hybrid element (CPE4RH) for a total simulated area: 384μm×192μm (thickness×width). As for boundary conditions of the plane strain model, the applied surface tractions correspond to the applied pressure on the shocked surface. At the bottom surface, the vertical displacement is specified as zero and the outer edges are traction free. The pressure distribution on the surface follows a Gaussian as $P(x) = P_0 \exp\left(-\frac{x^2}{2R^2}\right)$, where x is the radial distance from the center of the laser beam and R is the radius of plasma, which is assumed to be equal to 6μm here. The peak value of pressure is assumed to be $P_0/\tau_{CRSS} = 7$.

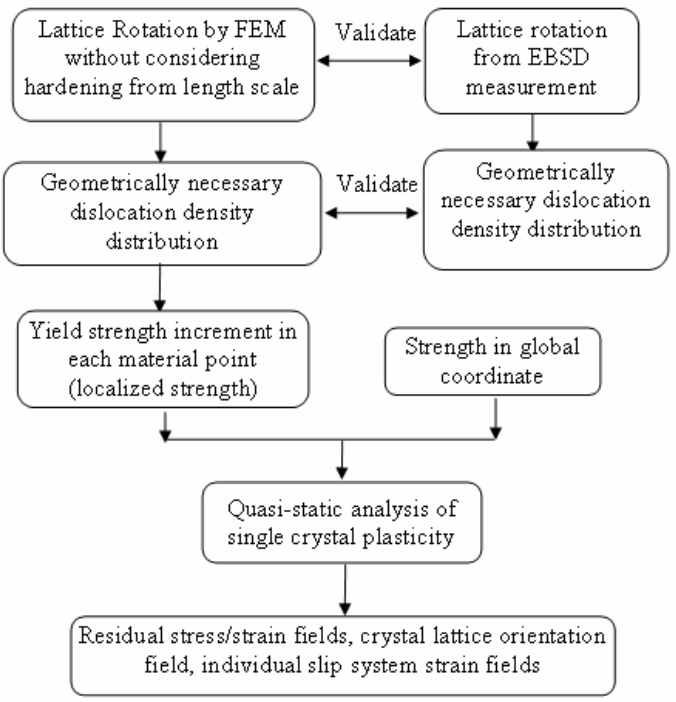

Fig. 5 The scheme FEM simulation of spatially resolved GND dependent deformation

RESULTS AND DISCUSSION

Lattice rotation field

From the measurement mentioned above, the resulting lattice rotation due to laser shock peening was obtained. In order to measure the lattice rotation below the sample surface and study the spatial distribution in the depth direction, the sample was sectioned on a (110) plane via wire EDM and the crystallographic orientation of the newly exposed surface was mapped using EBSD. The lattice rotation obtained in this manner is called "in-plane" because the experimental results indicate an approximate two-dimensional deformation state. Fig. 6 shows the lattice rotation in the cross section, which shows that the lattice rotation varies between ±2° in the region up to 60μm below the sample surface. In the center of the shock line, the lattice rotation is nearly zero (green) and rotation direction reversed across the shocked line, which is consistent with the result from sample surface. The maximum lattice rotation occurs near the sample surface and the value decays as depth increases. The lattice rotation from FEM simulation shown in Fig. 7 indicates two distinct misorientation regions on each side which is similar to the EBSD result. Also, there is a misorientation free region in the middle which can be seen from the experimental result as well. It can be seen from lattice rotation field of EBSD measurement that the plastic deformation zone is about 100μm while FEM simulations predict a 50μm zone. This may be due to lateral expansion of plasma as this effect is a more significant concern for a small beam size [1]. Also, in the simulation quasi-static loading is assumed and the peak pressure is only 7MPa, but in microscale LSP, the peak pressure is usually above 2GPa [1].

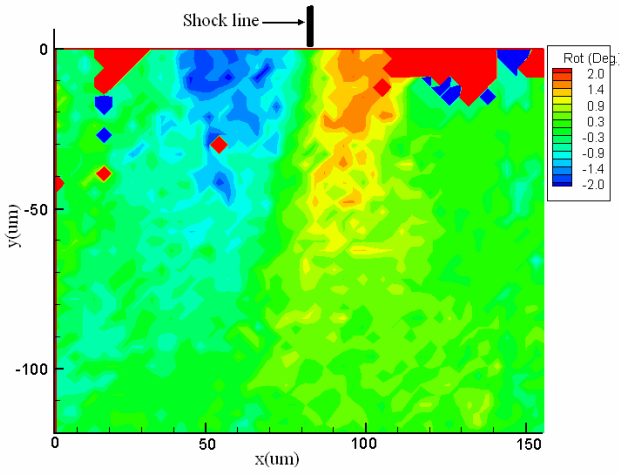

Fig. 6 Crystal lattice rotation by EBSD measurement

Geometrically necessary dislocation density (GND) and its hardening

Geometrically necessary dislocation density Based on the evaluation principles of GND, its distribution can be found from both simulation and experiments for the shocked specimen. Fig. 8 shows the geometrically-necessary dislocation density from the EBSD measurements. It can be seen that the magnitude of GND is about 9×10^{13} m^{-2}, which is coincident with large lattice rotation and the rotation free region at the shock line center. The distribution consists approximately of three regions, denoted as A, B and C, corresponding to the blue area (negative rotation), green area (zero rotation) and red area (positive rotation) of lattice rotation field in Fig. 6. The geometrically-necessary dislocation density by FEM simulation is shown in Fig. 9. It indicates that the magnitude of GND is about 1.4×10^{14} m^{-2}, which is almost twice of the experimental result. This is due to the plastic deformation size predicted by FEM is only half of the experiment but the magnitudes of rotation are almost same. Similarly, GND contour from FEM simulation can be divided into three distinctive regions, corresponding to the experimental result of A, B, C region. Compared with the experiment, the GND distribution area By FEM is quite smaller. This is again due to the assumptions in the simulation, such as quasi-static loading and no radial expansion of plasma. From the contour of lattice rotation by both experiment and FEM simulation, the green area (transition zone from negative lattice rotation to positive lattice rotation) has the maximum dislocation though the rotation is about zero. This is because the lattice rotation mismatch is most pronounced in this area. In order to preserve lattice compatibility in the case of unevenly distributed plastic slip, a large GND dislocation will be accumulated.

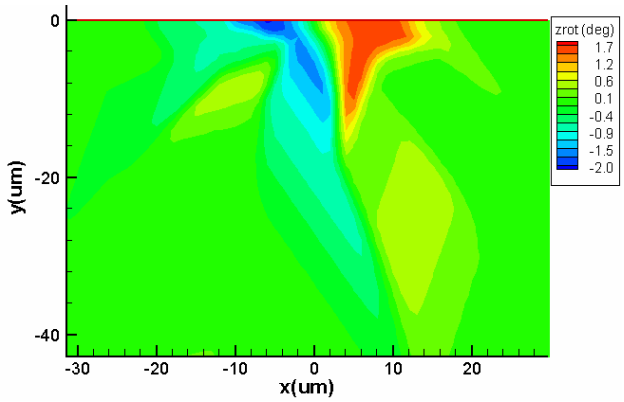

Fig. 7 Crystal lattice rotation by FEM simulation without considering length scale effects

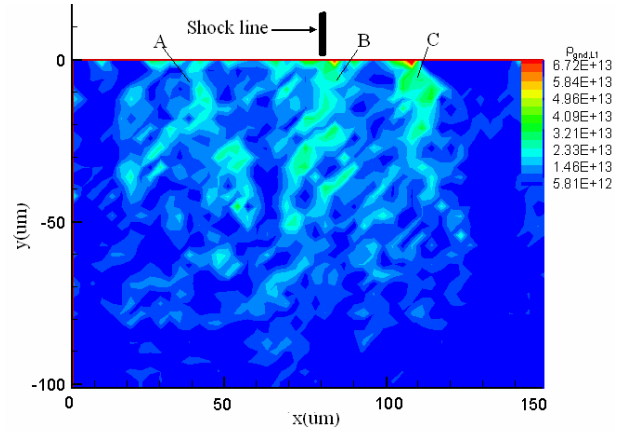

Fig. 8 The distribution of geometrically necessary dislocation density (in m^{-2}) from EBSD measurement, corresponding to Fig. 6

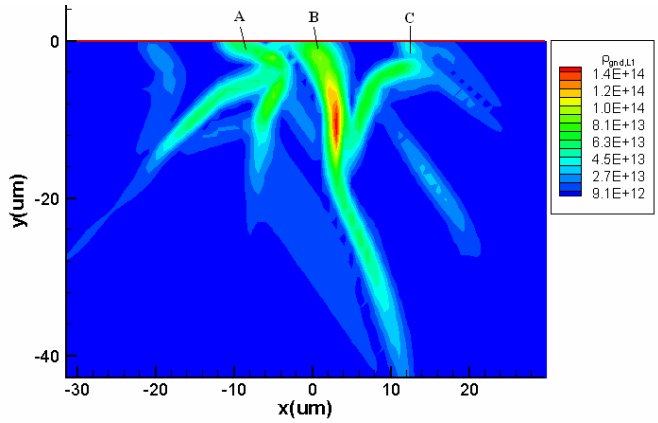

Fig. 9 The distribution of geometrically necessary dislocation density (in m^{-2}) from FEM simulation, corresponding to Fig. 7

Fig. 10(b)-(d) give the geometrically necessary dislocation density by FEM in each active slip system as shown in Fig. 10(a). A detailed description of three slip systems under plane strain condition can be found in [18]. It can be seen from Fig. 10 that GND in slip system *i* have the biggest magnitude and that of slip system *iii* is the weakest among the three. The difference can be explained by considering the Schmidt factor in each active slip system. Suppose the loading direction is *l*, the slip plane normal is *n*, the slip direction is *s*, the Schmidt factor can be represented as $\cos\phi \times \cos\lambda = (n \cdot l) \times (s \cdot l)$, where ϕ is the angle between *n* and *l* and λ is the angle between *s* and *l*. From Fig. 10(a), we can find that Schmidt factor for slip system *i*, *ii* and *iii* is 0.472, 0.315 and 0.263, respectively. Therefore, GND in slip system *i* is greater than that of slip system *ii*; and slip system *ii* is larger than slip system *iii*. Beside the spatial distribution, temporal evolutions for both lattice rotation and GND were presented in Fig. 11 for four different material points. The material point of node 1 corresponds to the origin (0, 0), which is located on the top surface at the shock line center. The material point of node 3 (3μm, -10μm) corresponds to the largest GND, which is located 10μm below the top surface and 3μm right from the shock line center. The other two points are randomly selected. From Fig. 11, we can see that GND increases almost linearly after a very short time 0.1 second and has no direct relationship with the time history of lattice rotation. For the origin (0, 0), the lattice rotation remains almost zero, but GND in this point increases constantly.

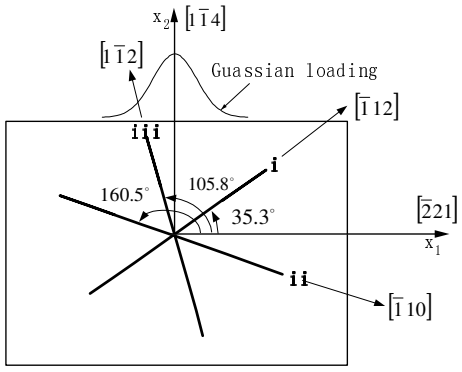

(a)

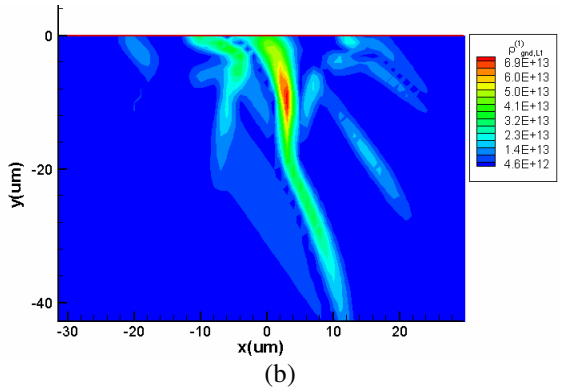

(b)

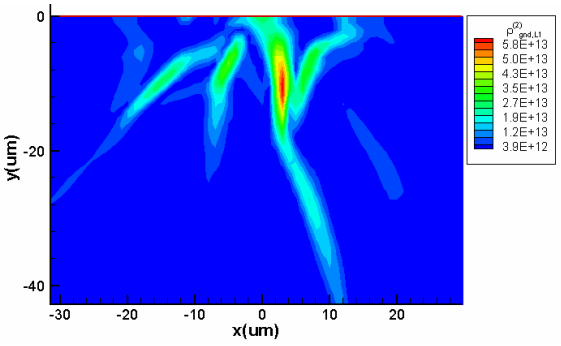

(c)

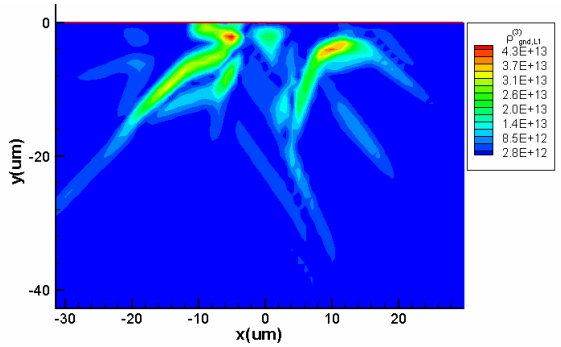

(d)

Fig. 10 a) Plane strain slip systems corresponding to $(1\,\bar{1}\,4)$ orientation; and GND distribution in each slip system (in m^{-2}) by FEM simulation: b) in slip system *i*; c) in slip system *ii*; d) in slip system *iii*

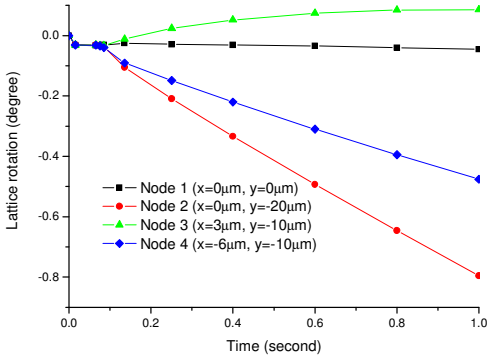

(a)

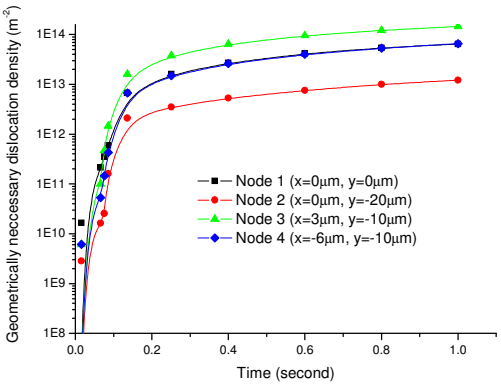

(b)

Fig. 11 Temporal evolution for four discrete material points of a) lattice rotation and b) geometrically-necessary dislocation density

Comparison with conventional indentation Compared with laser shock peening, geometrically-necessary dislocation density has been well studied in the conventional indentations [3, 12, 19, 20]. Furthermore, lattice rotation of indentation is relative large. Therefore, it is interest to compare laser shock peening with indentation to get some idea of the extent of the effects of GND.

The following shows the comparison with the work by Kysar et al. [12] for wedge indentation. In their work, wedge indention was performed on aluminum single crystal specimens with a wedge apex angle of 90°. The indenter was made of tungsten carbide bonded by a ferrous alloy. The indentation process was under the load control condition using a materials testing system (MTS 810) with a 548 controller. The loading direction was along [001] crystallographic orientation and the indenter axis were parallel to the [110]. The magnitude of in-plane lattice rotation ranges from -10° to 10° and the plastic deformation zone is quite large, which is about 500μm (depth) × 400μm (width). The magnitude of lattice rotation is about 5 times of that by laser shock peening while the average GND density is about 1×10^{14}m^{-2} for the indentation and about 5×10^{13}m^{-2} for μLSP, which is half of the indentation. Thus, though the magnitude of lattice rotation is relatively small for μLSP comparing with the indentation, the GND density is still comparable with that of the indentation. Therefore, like in the indentation, length scale effects are also needed to be considered in μLSP.

GND Enhanced strength distribution In order to integrate the GND hardening into FEM simulation, the yield strength increment for each slip system under plane strain condition must be calculated from the GND distribution of each slip system based on Eq. (7). For a FCC crystal, the Burgers vector is $\mathbf{b}=\frac{a}{2}[110]$ and the magnitude is

$$|\mathbf{b}|=\frac{a}{2}(h^2+k^2+l^2)^{1/2}=\frac{\sqrt{2}}{2}a \qquad (8)$$

where α is the lattice constant, which is 0.405nm for aluminum. Thus the magnitude of Burgers vector is b = 0.28 nm for single crystal aluminum. By projecting Burgers vector into the activated slip system, the effective length of Burgers vector of each slip system can be found. From Kysar et al. [18] and Wang et al.[21], only three slip systems should be considered under the plane strain condition. Slip system *i*, $(1\bar{1}1)[\bar{1}12]$, is the combination of $(1\bar{1}1)[011]$ and $(1\bar{1}1)[\bar{1}01]$, slip system *ii* is the combination of slip systems $(111)[\bar{1}10]$ and $(11\bar{1})[\bar{1}10]$, and slip system *iii*, $(\bar{1}11)[1\bar{1}2]$, is the combination of $(\bar{1}11)[101]$ and $(\bar{1}11)[0\bar{1}1]$. By geometry, the effective lengths of Burgers vector are $\frac{\sqrt{3}}{2}|\mathbf{b}|$, $|\mathbf{b}|$ and $\frac{\sqrt{3}}{2}|\mathbf{b}|$ for the three slip systems, respectively.

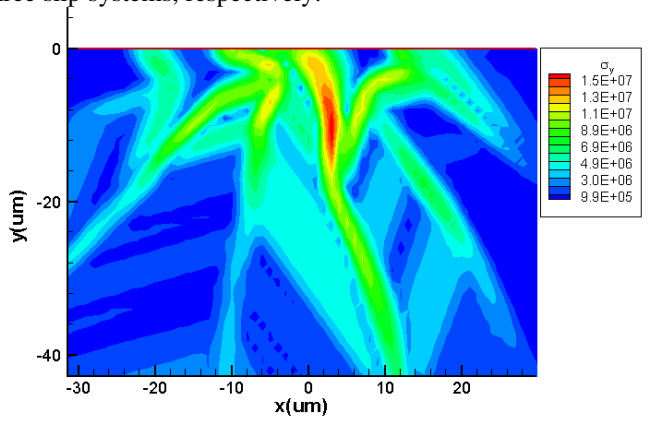

Fig. 12 Hardening by geometrically necessary dislocation density (in Pa)

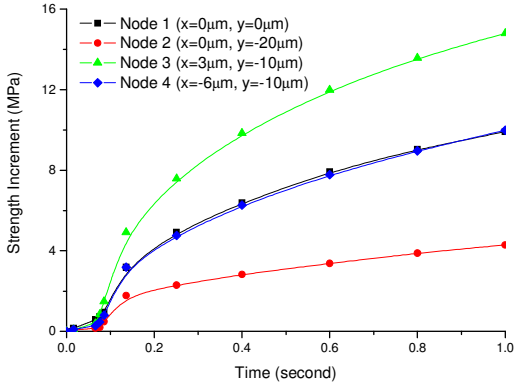

Fig. 13 Temporal evolution for four discrete material points of strength increment by geometrically necessary dislocation density

Fig. 12 shows the results of hardening by geometrically necessary dislocation density for three slip systems. It can be seen that the magnitude of the enhanced strength is about 15MPa and the effected area is around 40μm×60μm. Beyond that area, there is almost no length scale effect. Thus length scale effects are localized and also vary within this area. According to the Schmid law, the slip system starts to glide when τ^k reaches the critical shear stress of the crystal τ_0. This

glide causes plastic deformation of the crystal. Shear stress on this active slip system is kept at τ^k as long as the slip system is gliding. Due to hardening caused by geometrically necessary dislocation density, the material is difficult to deform.

Effects of GND hardening by FEM results

In FEM simulation, the strength increment of each material point as shown in Fig. 12 was implemented at the corresponding node for each slip system during the loading step and kept constant during the unloading step. Initially, the strength increment is zero and increases linearly to the maximum at the end of the first step. This agrees quite well with the time history of strength increment as shown in Fig. 13. Also, the simulation parameters, such as the loading pressure, element type and mesh size, etc. are kept the same before and after consideringt GND hardening.

Fig. 14 shows the comparison of normal displacement of the shocked surface. It is found by SPM measurement that the deformation is approximately uniform along the shocked line, which is indicative of a 2-D deformation state. The detailed cross section profile in Fig.14 shows that the deformation depth is about 2μm and plastic deformation size is about 125μm. Without the GND hardening, the magnitude is 3.75μm by FEM with the assumptions of quasi-static loading with a fixed plasma radius. Through the implement of the yield increment by GND, the magnitude of the normal displacement is reduced to 2μm, which is the same as the SPM measurement. However, the only conclusion that may be drawn is the hardening caused by GND plays an important role in plastic deformation and can not be ignored.

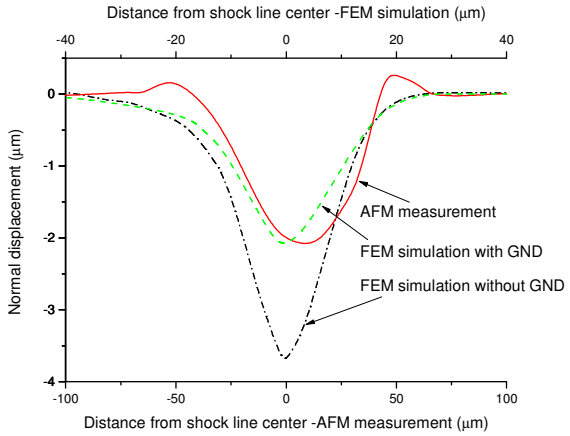

Fig. 14 Comparison of normal displacement of the shocked surface by FEM with length scale effects and without considering length scale effects

Fig. 15 (a)-(b) show the total shear strain distribution, the summation of shear strain in three slip systems, in the cross-section for both cases. The magnitude of the case without considering the GND hardening is about 6.6% and 3.7% for the simulation with the GND hardening term. In addition, there is almost no plastic deformation in the two side regions for the case with GND hardening. According to anisotropic slip line theory [13], the Gaussian loading can be approximated as a non-uniform "punch" and the plastic deformation zone can be divided into three regions. One is right beneath the "punch", the other two are on the two sides, respectively. For details, one can refer to the work by Wang, et al.[21]. In these three regions, only slip system *iii* is active. The stress status in these two side regions has $\sigma_{11}/\tau_0 = -\sqrt{6}$, $\sigma_{22}/\tau_0 = 0$ and $\sigma_{12}/\tau_0 = 0$, where direction 1 is along the surface and direction 2 is perpendicular to the surface. Because τ_0 is increased along the time quickly in the case considering GND hardening, the yield surface will expand and τ_0 will exceed σ_{11} at some point in time. If the shear stress is smaller than τ_0, the slip system does not glide, and only elastic deformation is possible. Thus, there is almost no plastic deformation in the two side regions Q and H.

Comparison of GND hardening and statistically stored dislocation (SSD) hardening

The hardening caused by SSD includes self hardening and latent hardening and occurs in both macro- and micro- worlds. It has been well investigated and is basic to the constitutive crystal plasticity framework [22]. Usually, the local continuum constitutive models implicitly assume that the accumulation of SSD is the only driving force behind work hardening. Thus, it is of interest to compare the hardening effects caused by SSD and GND.

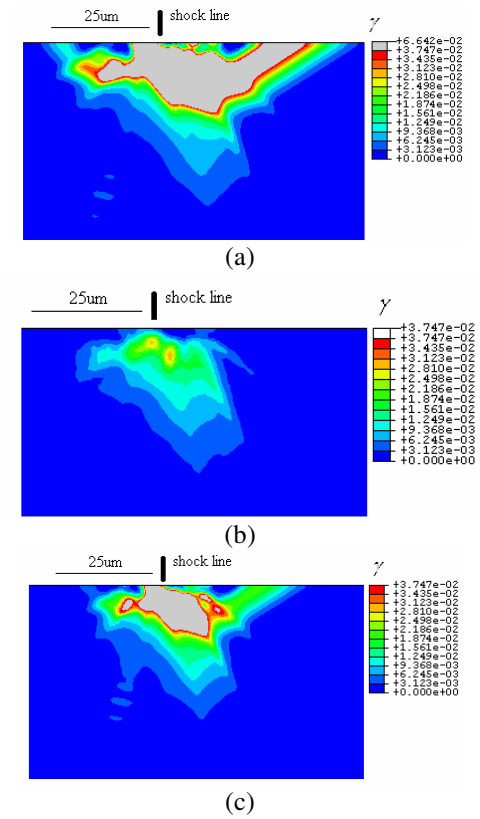

Fig. 15 Total shear strain distribution: a) without considering length scale effects; b) only considering length scale effects; and c) only considering the hardening of statistically stored dislocation

In the simulation considering SSD hardening, Asaro's hardening theory of single crystal [14] has been applied, in which the critical shear stress τ_0^k of the Schmid law is determined by the current SSD and represents variation of hardness of material due to work hardening by SSD. Since work hardening of the slip system depends on shear deformation of the slip systems, the variation of τ_0^k may be estimated by

$$\Delta\tau_0^k = \sum_i h_i^k |\Delta\gamma_i| \quad (9)$$

where h_i^k expresses hardening rate against increment of shear deformation $\Delta\gamma_i$ on each slip system. When *k* equals *i* and h_i^k represents hardening by glide on its own slip system. When *k* does not equal *i*, h_i^k represents hardening by glide on other slip systems. The former is called self hardening, and the latter is called latent hardening. The values of h_i^k can be found in Wang et al. [21].

Fig. 15 (c) shows the FEM result for the total shear strain distribution considering of only SSD hardening. It is seen that the magnitude is close to that of GND hardening. Also, the spatial distribution is comparable with that without any hardening; that is, slip system *iii* is active in both regions H and Q.

CONCLUSIONS

In this study, length scale effects for micro scale laser shock peening on a single crystal aluminum with orientation $[1\bar{1}4]$ are investigated with EBSD measurement and FEM simulation with single crystal plasticity. Given the laser beam size at 12μm with intensity of 4GW/cm^2, EBSD measurement shows that the induced crystal lattice rotation is about ±2°. The magnitude of the corresponding geometrically necessary dislocation density is 9×10^{13}m^{-2}. The spatial distribution of the geometrically necessary dislocation density shows the density right underneath the shock center surface is high though the lattice rotation is close to zero. In addition, the GND induced by μLSP is comparable with that of the conventional indentation induced severe plastic deformation, which has a rotational magnitude of 10°. The average GND density is about 1×10^{14}m^{-2} for the indentation while it is about 5×10^{13}m^{-2} for μLSP. By implementing the GND hardening into FEM simulation, it is found that length scale effects can not be neglected. The plastic deformation size is significantly decreased after considering GND hardening; from 80μm to 30μm. From the spatial total shear strain distribution, the plastic deformation is mainly concentrated right underneath the "punch". Beyond the "punch" radius, there is almost no plastic deformation. Also, the comparison with the hardening effects of SSDs shows that these two hardenings are comparable with each other. The experimental methodology and results of the work present a systematic study of the length scale effects for the micro scale laser shock peening process. It is now possible to integrate length scale effects into the single crystal based FEM model to conduct more realistic simulation for the micro scale LSP process.

ACKNOWLEDGMENTS

This work is supported by the National Science Foundation under grants DMI-02-00334 and DMI-06-20741. JWK would like acknowledge support by the National Science Foundation under the Faculty Early Career Development (CAREER) Program with grant CMS-0134226. Single crystal sample preparation provided by Dr. Yongxue Gan is also acknowledged.

REFERENCES

[1] Zhang, W., and Yao, Y. L., 2001, "Micro-scale Laser Shock Processing: Modeling, Testing, and Microstructure Characterization," *SME J. of Manufacturing Processes*, Vol. 3, No.2, pp. 128-143

[2] Chen, H., Kysar, J., and Yao, Y. L., 2004, "Characterization of Plastic Deformation Induced by Micro Scale Laser Shock Peening," *ASME Trans. J. of Applied Mechanics,* Vol.71, No.3, pp.713-723

[3] Ma, Q. and Clarke, D.R., 1994, "Size Dependent Hardness of Silver Single Crystals", *Acta Metallurgica et Materialia*, v 42, n 5, pp. 1673-1681.

[4] Stolken, J.S. and Evans, A.G., 1998, "Microbend test method for measuring the plasticity length scale," *Acta Materialia* 46, pp. 5109-5115

[5] Dai, H., Parks, D.M., 1997, "Geometrically necessary dislocation density and scale-dependent crystal plasticity", In: Khan, A.S. (Ed.), Proceedings of Plasticity '97: The Fifth International Symposium on Plasticity and its Current Applications. Neat Press, Juneau, Alaska, pp. 17–18.

[6] Arsenlis, A. and Parks, D.M., 1999, "Crystallographic aspects of geometrically-necessary and statistically-stored dislocation density," *Acta Materialia*, v 47, n 5, pp. 1597-1611.

[7] Evers, L. P., Parks, D. M., Brekelmans, W. A. M., and Geers, M. G. D, 2002, "Crystal plasticity model with enhanced hardening by geometrically necessary dislocation accumulation," *Journal of the Mechanics and Physics of Solids* 50, pp. 2403-2424.

[8] Nye, J.F., 1953, "Some geometrical relations in dislocation solids", *Acta Metallurgica* 1, pp. 153-162.

[9] Ashby, M.F., 1970, "The deformation of plastically non-homogeneous materials," *Philosophical Magazine* 21, pp. 399–424.

[10] Gao, H., Huang, Y., Nix, W.D., Hutchinson, J.W., 1999, "Mechanism-based strain gradient plasticity - I. Theory," *Journal of the Mechanics and Physics of Solids*, v 47, n 6, pp. 1239-1263

[11] Sun, S., Adams, B.L., and King, W.E., 2000, "Observations of Lattice Curvature Near the Interface of a Deformed Aluminum Bicrystal," *Philosophical Magazine A: Physics of Condensed Matter, Structure, Defects and Mechanical Properties*, v 80, n 1, pp. 9-25

[12] Kysar, J.W., Gan, Y.X., Morse, T.L., Chen, X,. and Jones, M.E., 2007, "High Strain Gradient Plasticity Associated with Wedge Indentation into Face-centered Cubic Single Crystal: Geometrically Necessary Dislocation Densities," *Journal of the Mechanics and Physics of Solids*, 55, pp.1554-1573.

[13] Rice, J. R., 1973, "Plane strain slip line theory for anisotropic rigid/plastic materials", *Journal of the Mechanics and Physics of Solids*, 21, 63-74.
[14] Asaro, R. J., 1983, "Crystal Plasticity," *Journal of Applied Mechanics* 50, pp. 921-934.
[15] Huang, Y., 1991, "A user-material subroutine incorporating single crystal plasticity in the ABAQUS finite element program," Mech Report 178, Division of Applied Sciences, Harvard University, Cambridge, MA.
[16] Kysar, J.W., 1997. Addendum to "A user- material subroutine incorporating single crystal plasticity in the ABAQUS finite element program, Mech Report 178", Division of Engineering and Applied Sciences, Harvard University, Cambridge, MA
[17] Kysar, J.W., 2001. Continuum simulations of directional dependence of crack growth along a copper/sapphire bicrystal interface: Part I, experiments and crystal plasticity background. J. Mech. Phys. Solids 49, 1099–1128.
[18] Kysar, J. W., Gan, Y.X., Mendez-Arzuza, G., 2005, "Cylindrical void in a rigid-ideally plastic single crystal I: anisotropic slip line theory solution for face-centered cubic crystals", *International Journal of Plasticity*, 21, 1461-1657.
[19] Durst, K., Backes, B., Goken, M., 2005, "Indentation size effect in metallic materials: Correcting for the size of the plastic zone", *Scripta Materialia*, v 52, n 11, pp. 1093-1097
[20] Stelmashenko, N.A., Walls, M.G., Brown, L.M., Milman, Y.V., 1993 "Microindentation on W and Mo oriented single crystals: an STM stud," *Acta Metall. Mater*. 41, 2855–2865.
[21] Wang, Y., Kysar, J. W., and Yao, Y. L., 2008 "Analytical solution of anisotropic plastic deformation induced by micro-scale laser shock peening," *Mechanics of Materials*, 40, 100-114.
[22] Kalidindi, S.R., Bronkhorst, C.A., Anand, L., 1992, "Crystallographic texture evolution in bulk deformation processing of fcc metals," *J. Mech. Phys. Solids* 40, pp.537-569

.